Redox Biology 65 (2023) 102836

Contents lists available at ScienceDirect

Redox Biology

journal homepage: www.elsevier.com/locate/redox

Mechanism of action of platinum nanoparticles implying from antioxidant to metabolic programming in light-induced retinal degeneration model

Lin Su [a], Xiaoqun Gong [b,***], Ruiyan Fan [a], Tianwen Ni [a], Fuhua Yang [a], Xiaomin Zhang [a,**], Xiaorong Li [a,*]

[a] Tianjin Key Laboratory of Retinal Functions and Diseases, Tianjin Branch of National Clinical Research Center for Ocular Disease, Eye Institute and School of Optometry, Tianjin Medical University Eye Hospital, No. 251, Fukang Road, Nankai District, Tianjin, 300384, China
[b] School of Life Sciences, Tianjin Engineering Center of Micro-Nano Biomaterials and Detection-Treatment Technology, Collaborative Innovation Center of Chemical Science and Engineering, Tianjin University, Tianjin, 300072, PR China

ARTICLE INFO

Keywords:
Photoreceptors degeneration
Oxidative stress
Platinum nanoparticles
Retinal diseases

ABSTRACT

Photoreceptors (PRs) degeneration is central to visual impairment and loss in most blind retinal diseases, including age-related macular disease (AMD) and diabetic retinopathy (DR). PRs are susceptible to oxidative stress owing to their unique metabolic features. Accumulating evidence has demonstrated that the targeting oxidative stress is a promising treatment strategy for PR degeneration. Herein, we introduced potent anti-oxidative platinum nanoparticles (Pt NPs) to treat PRs degeneration in this study. The Pt NPs exhibited multi-enzymatic antioxidant activity and protected PRs from H_2O_2-induced oxidative damage *in vitro* assays. Based on the same mechanism, the intravitreal injection of Pt NPs significantly reduced cell apoptosis, maintained retinal structure and preserved retinal function in a mouse model of light-induced retinal degeneration (LIRD). Most importantly, the results of RNA sequencing showed that the transcription of antioxidative genes was upregulated, and metabolic reprogramming occurred in the LIRD-retina after treatment with Pt NPs, both of which benefited retinal survival from oxidative damage. The results indicated that Pt NPs were indeed potent therapeutic candidates for PRs degeneration in blind retinal diseases.

1. Introduction

The retina is a highly specialized tissue with a multilayered architecture and is an extension of the central nervous system [1,2]. Photoreceptors (PRs), located in the innermost region of the retina, are the first sensory neurons that enable vision. Within PRs, a more active metabolism than that of general neurons is required in response to high energy demands because of phototransduction, daily renewal of the outer segments of PRs, and maintenance of membrane potential in darkness [3,4]. Thus, reactive oxygen species (ROS), an inevitable by-product of metabolism, are produced frequently in PRs [5]. Once ROS production exceeds the intrinsic antioxidant capacity, oxidative stress occurs, resulting in a series of biological responses of the pathogenesis. Therefore, PRs are vulnerable to oxidative stress and are the major contributors to oxidative stress in the retina [5–7].

PRs degeneration is central to visual impairment and loss in many blind retinal diseases including age-related macular disease (AMD), diabetic retinopathy (DR) and retinitis pigmentosa (RP). Irrespective of the initiating defect, oxidative stress accelerates the degeneration of RPs both at the beginning and during progression [8,9]. Meanwhile, increasing evidence demonstrate that targeting oxidative stress is a promising treatment strategy for PRs degeneration [2,10,11]. Unfortunately, clinical therapeutic options of PRs degeneration remain suboptimal; therefore, there is an urgent unmet need for therapies that can improve PR survival and ultimately, vision.

In recent years, nanomaterials with enzyme-like activities, also called nanozymes, such as platinum, cerium or fullerene nanoparticles, have attracted a wide range of applications in nanomedicine [12–14]. In particular, interest in platinum nanoparticles (Pt NPs) is rapidly growing because they possess multi-enzymatic activities to scavenge ROS [12,15]. Notably, Pt NPs not only catalyzed the decomposition or reduction of H_2O_2 acting as intrinsic enzyme peroxidase (POD) and catalase (CAT)

* Corresponding author.
** Corresponding author.
*** Corresponding author.
E-mail addresses: gongxiaoqun@tju.edu.cn (X. Gong), xzhang08@tmu.edu.cn (X. Zhang), lixiaorong@tmu.edu.cn (X. Li).

https://doi.org/10.1016/j.redox.2023.102836
Received 7 July 2023; Received in revised form 24 July 2023; Accepted 31 July 2023
Available online 1 August 2023

mimics, respectively, but also catalyzed the dismutation of O_2^- into O_2 and H_2O_2 as superoxide dismutase (SOD). Encouraging results from nanomedical research indicate that Pt NPs are promising candidates for treating oxidative stress-related diseases [16–20].

We hypothesized that the engineered Pt NPs could counter intracellular ROS and protect the retina, especially the PRs, from oxidative damage. To test this, we conducted a series of experiments with *in vitro* cell system and *in vivo* light-induced retinal degeneration model of albino mice. All the results indicated that Pt NPs were potent therapeutic candidates for PRs degeneration in blind retinal diseases.

2. Materials and methods

2.1. Materials

Pt nanoparticles were purchased from Nanjin XFNANO Materials Technology Co. Ltd. (Nanjing, China). TMB single color liquid, 2′,7′-dichlorofluorescein diacetate (DCFH-DA) were bought from Beijing Solarbio Science &Technology Co., Ltd. (Beijing, China). MitoSox Red was purchased from Thermo Fisher Scientific (USA). Dulbecco's Modified Eagle Medium (DMEM), trypsin-EDTA (100 ×), and Penicillin-Streptomycin Solution (100 ×) were obtained from Gibco Life Technologies (Grand Island, NY, USA). Fetal bovine serum (FBS) was obtained from HyClone (Boston, MA, USA). H_2O_2, Crystal Violet Staining Solution, Total Superoxide Dismutase Assay Kit with NBT, One Step TUNEL Apoptosis Assay Kit (Red Fluorescence), 4% paraformaldehyde, Autophagy Staining Assay Kit with MDC, 0.3% triton X-100 was from Beyotime Biotechnology Co., Ltd (Beijing, China). Salicylic acid (SA) was obtained from Aladdin. The Cell Counting Kit-8 was purchased from Dojindo Laboratories (Kumamoto, Japan). The antifade mounting medium containing DAPI was purchased from Vector Laboratories, Inc. (Burlingame, CA, USA).

2.2. Animals

Six to eight weeks of BALB/c mice were obtained from SPF (Beijing) Biotechnology Co., Ltd (Beijing, China). All procedures involving animals were performed in accordance with the ARVO statement for the use of Animals in Ophthalmic and Vision Research and Tianjin Medical University Eye Institute Guidelines for Animal Research. The mice were kept in a room with a 12/12 h light/dark cycle before the start of the experiment.

3. Methods

3.1. Characterization of Pt NPs

The morphology of the Pt NPs was characterized by transmission electron microscopy (TEM, Hitachi HT7700). A Zetasizer Nano system (Malvern ZS90) was used to measure the diameter and surface zeta potential of the Pt NPs in the solution.

3.2. CAT-like activity of Pt NPs

H_2O_2 has strong absorption at 240 nm. Therefore, a spectrophotometric method was used to determine the concentration of H_2O_2. Briefly, 3 mL of 10 mM H_2O_2 was used as a control. Pt NPs with final concentration of 0.4 and 4 mM in the same volume of H_2O_2 were used as the test groups. Every 10 min, all the solutions were tested using a UV–vis spectrophotometer (UV-2450, Shimadzu). The absorbance of each sample solution diluted with water was used as a blank.

3.3. POD-like activity of Pt NPs

A TMB single-color liquid and H_2O_2 were used to test the POD-like activity of the Pt NPs. The POD enzyme catalyzes H_2O_2 to oxidize colorless TMB to blue. 100 μL of TMB and 100 μL of water were used as negative control. 100 μL of TMB, 50 μL of 1 M H_2O_2, and 50 μL of water were also used as control. 100 μL of TMB, 50 μL of 1 M H_2O_2, and 50 μL of Pt NPs solution were mixed as experimental groups. The final concentrations of the Pt NPs in the final liquid were 0.05, 0.1, and 0.2 mM, respectively. All samples were immediately analyzed using an EnSpire Multilabel Reader (Perkin Elmer Instrument Co., Ltd., USA) with a preset procedure (absorbance at 652 nm, shaking for 10 s between each cycle, 30 min for 30 cycles). The absorbance was positively correlated with the POD-like activity of the Pt NPs.

3.4. SOD-like activity of Pt NPs

The SOD-like activity of Pt NPs was tested using Total Superoxide Dismutase Assay Kit as described in the manufacturer's instructions. Briefly, the NBT working solution was prepared using SOD buffer, NBT liquid, and enzymes. The starting solution was prepared using the reaction solution (40 ×) and SOD buffer. All the chemicals were provided by the manufacturer. Pt NPs testing samples with gradient concentrations (0.1, 0.2, 0.4, 1.6 mM) were made in a total volume of 200 μL. Samples without Pt NPs or starting solution were used as $blank_1$ and $blank_2$, respectively. The absorbance of all the samples was measured at 560 nm using EnSpire Multilabel Reader (PerkinElmer Instrument Co., Ltd., USA). The O_2^- generated in the sample solution turned the colorless NBT blue. The percent inhibition was positively related to the SOD-like activity of the Pt NPs and was calculated using the following formula:

$$\text{Inhibition percentage} = \text{SOD activity}\ (\%) = (\text{Blank}_1\text{-Sample}) / (\text{Blank}_1\text{-Blank}_2) \times 100$$

3.5. Fenton reaction assay

The $FeSO_4$ and H_2O_2 system is considered as a classic Fenton reaction model. The • OH generated in this system oxidizes SA to form 2,3-dihydroxybenzoic acid, which has a strong absorption at 510 nm. The absorbance is positively correlated with the Fenton reaction activity. To test whether the Pt NPs could produce •OH through the Fenton reaction, 1.8 mM SA was mixed with 1.8 mM $FeSO_4$ or a gradient of Pt NPs. The final concentrations of the Pt NPs in the solutions were 0.3, 1, and 50 mM. Next, 5 mM H_2O_2 was added and the mixture was incubated for 10 min at RT. Absorbance was measured using EnSpire Multilabel Reader (PerkinElmer Instrument Co., Ltd., USA). Next, the chemical stability of the Pt NPs was assessed by detecting possible iron release in the lysosomal mimic fluid. The Pt NPs were incubated in an acetate buffer at pH 3–4 for 24 h before being added to the testing solution. The absorbance of the acidic solution was also measured. The absorbance was positively correlated with the Fenton reaction activity.

3.6. Cell culture and cell cytotoxicity assay

661 W cells were routinely cultured in DMEM containing 10% FBS and 1 × Penicillin-Streptomycin Solution, at 37 °C in a humid environment with 5% CO_2. 661 W cells were seeded in 96-well plates at a concentration of 8000/well and incubated for 24 h before further experiments. To test the cytotoxicity, cells were incubated with gradient concentrations of Pt NPs (100, 200, 400 μM) for another 24 h and 48 h. The following procedures were performed according to the instructions of the Cell Counting Kit (CCK-8).

3.7. Protective effect of Pt NPs in cell model

H_2O_2 was used to induce oxidative stress in 661 W cells. Cells were plated as previously described. Medium containing 600 μM H_2O_2 was incubated with cells for 6 h, then fresh medium with different

concentrations of Pt NPs (0, 1, 3, and 10 nM in PBS solution) was changed and the cells were incubated for 18 h. The cell viability of each group was determined using CCK-8. To visualize cell morphology and number, crystal violet staining was performed according to the manufacturer's instructions. Briefly, cells were fixed with 4% paraformaldehyde (PFA) for 30 min. After washing three times with water, 1 × crystal violet solution was added for 30 min of staining. The plate was washed until the cells exhibited a definite morphology. The cells were photographed under a microscope. Image J software was used to calculate the relative cell numbers for each group.

3.8. Intracellular ROS scavenging of Pt NPs

H_2O_2 was used to induce elevated intracellular ROS levels. 661 W cells were seeded as previously described. Except for the normal cells, the residual cells were treated with 600 μM H_2O_2 for 4 h, fresh medium containing Pt NPs (0, 1, and 3 nM) was added, and the cells were incubated 16 h. Superoxide formation in live cells was imaged using MitoSox Red, and intracellular ROS were probed using a ROS assay kit, following the manufacturer's instruction. Briefly, the cells were washed and incubated with 5 μM MitoSox Red or 10 μM DCFH-DA in their respective buffer for 20 min at 37 °C. The cells were then washed three times. Fluorescence images of the cells were captured using a fluorescence microscope (MitoSox Red, excitation: 396 nm, emission: 610 nm). In addition, the cells stained with DCFH-DA were trypsinized and collected for flow cytometry to quantify ROS levels in each group (excitation: 488 nm, emission: 517 nm). The data were analyzed using FlowJo 7.6 analysis software.

3.9. Autophagosomes staining assay

Cells were treated with H_2O_2 as described above. The cells were washed and incubated with 1 × MDC in fresh medium for 30 min in the dark. After washing the cells with PBS, a fluorescence microscope (excitation: 335 nm; emission: 512 nm) was used to detect distinct dot-like structures representing autophagosomes. Image processing was performed using the Image J software.

3.10. TUNEL staining for cells

Cells were treated with H_2O_2 as described above. After washing three times with PBS, the cells were fixed with 4% PFA for 30 min, followed by three more washes. 0.3% Triton X-100 in PBS was used for cell permeation (10 min). After washing cells again, the one step TUNEL solution provided by the kit was added for staining at 37 °C for 1 h. Washing residual TUNEL solution with PBS for at least three times, the cells were sealed with antifade mounting medium with DAPI. A fluorescence microscope (excitation wavelength, 550 nm; emission wavelength, 570 nm) was used to detect TUNEL-positive cells. Image processing was performed using the ImageJ software.

3.11. Light-induced retinal degeneration model

Mice were kept in boxes for dark adaption for 16 h, followed by exposure to intense blue light for 1 h, and then returned to the dark 16 h. Before exposure to the blue light, tropicamide (0.5%) was topically applied to the cornea to dilate the pupils. A box with a blue ball on top and mirrors around the four sides was used for light induction. The illumination of the light in each corner of the box was approximately 2000 lux. When light exposure of 1 h was finished, intravitreal injection of Pt NPs with different concentrations (0.3 and 1 μM in PBS solution) in a volume of 1 μL were subsequently performed. Equivalent volumes of vehicle (PBS) were administered to part of the Light-induced retinal degeneration (LIRD) mice. Mice without LIRD but injected with 1 μL of vehicle were used as normal group.

3.12. Electroretinogram (ERG)

ERG testing were conducted 3 days after light exposure. Dark-adapted mice were anesthetized with ketamine (35 mg/kg) and xylazine (5 mg/kg), and the pupils were dilated as previously mentioned. Scotopic ERGs in different groups were recorded using an electrophysiological system (Ganzfeld, Phoenix Research Laboratories, USA) in a masked manner. A green light with an intensity of 3.1 log cd sec/m^2 was used for the ERG response. Eight sweeps were recorded at 30 s intervals for each eye.

3.13. Optical coherence tomography (OCT)

OCT imaging was performed immediately after ERG recording. Mice were anesthetized and the pupils were dilated as previously mentioned. OCT (Heidelberg Engineering, Heidelberg, Germany) was used to observe retinal structures. An ART scanning model with two crossing directions and a dense scanning model were selected, and OCT system software was used to calculate the thickness of the layers of the retina.

3.14. Hematoxylin and eosin (H&E) staining and TUNEL for retina

Following the OCT image acquisition at day 3, animals were sacrificed and the eyes were enucleated, fixed in 4% PFA, and embedded in paraffin. Paraffin sections (4 μm) crossing the optic nerve were stained with H&E. For TUNEL staining, paraffin sections (6 μm) were dewaxed and subjected to one-step TUNEL staining, as described in the manufacturer's instructions. Photographs of these sections were taken using a microscope to observe the retinal structures and apoptotic cells. The images were processed using Image J.

3.15. RNA sequencing and data analysis

The retinas were collected at day 2 after light-induced retinal degeneration. The mice were divided into 3 groups, normal group, vehicle group and Pt NPs group. The mice without light-induction but injected with vehicle were set as normal group, the light-induced mice injected with vehicle were named as Vehicle and the light-induced mice injected with Pt NPs (1 μM in a volume of 1 μL) were named as Pt NPs group. Four retinas from different mouse belonging to the same group were pooled and considered as one sample, and each group had three replicate samples. RNA sequencing experiments and patterned data processing were performed by Wuhan Yingzi Gene Technology Co., Ltd. Genes with a fold change >1.5 and $p < 0.05$ were regarded as differentially expressed. Raw sequence reads were available, if required. Genes and pathways of interest were identified using Sangerbox tool.

3.16. RNA isolation and RT-PCR

The retinas were collected in the same way that performed in the RNA sequencing part. The total mRNA were extracted using an Universal RNA Purification Kit (EZBioscience, USA) according to the manufacturer's. Then the mRNA (1 μg) were reversed into cDNA using Color Reverse Transcription Kit (EZBioscience, USA). RT-PCR was conducted using LightCycler®480 (Roche, Switzerland). The primer sequences used for PCR were shown in Table 1. The reaction conditions were 95 °C for 5 min followed by 40 cycles of 95 °C for 15 s and 58 °C for 30 s. β-actin was used as an internal control to normalize the expression of target gene. Relative expression was calculated using the $2^{-\Delta Ct}$ method [21].

3.17. Statistical analysis

Data of thickness of ONL in animal model (Fig. 5) was shown as mean ± SEM, the other experiment data were shown as mean ± SD. Statistical differences among groups were determined using one-way analysis of

Table 1
PCR primers of the detected mRNAs.

Gene name	Forward	Reverse
Pi3kca	CCACGACCATCTTCGGGTG	ACGGAGGCATTCTAAAGTCACTA
Akt3	TGGGTTCAGAAGAGGGGAGAA	AGGGGATAAGGTAAGTCCACATC
Ep300	TTCAGCCAAGCGGCCTAAA	CGCCACCATTGGTTAGTCCC
Pgd-1	ATGGCTGGCAAGAAAGTCTG	CGTGCTGAGTGTTGATGATCT
Tkt	ATGGAAGGTTACCATAAGCCAGA	TGCAGCATGATGTGGGGTG
Gapdh	AGGTCGGTGTGAACGGATTTG	TGTAGACCATGTAGTTGAGGTCA
Sod3	CCTTCTTGTTCTACGGCTTGC	TCGCCTATCTTCTCAACCAGG
Gpx1	AGTCCACCGTGTATGCCTTCT	GAGACGCGACATTCTCAATGA
Gstk1	GGTCCTATGCAGATACCAACAC	GTACTGGCCTTTTCGGGGAA
β-actin	GGCTGTATTCCCCTCCATCG	CCAGTTGGTAACAATGCCATGT

variance (ANOVA). Differences were considered statistically significant at $p < 0.05$.

4. Results and conclusions

4.1. Characterization of Pt NPs

The Pt NPs were well dispersed, and most of them were approximately smaller than 5 nm, as shown in the TEM image (Fig. 1A). The size distribution of the Pt NPs and the zeta potential were identified using DLS measurements. Surface zeta potential of the Pt NPs was negative with a value of -0.47 ± 0.1 (mV) and over 60% of the Pt NPs in the solution was about or smaller than 10 nm (Fig. 1B). The hydrodynamic diameters measured using DLS were always larger than those measured using TEM.

4.2. Multi-enzymatic activities of PtNPs

Despite the various kinds of ROS, the impact of H_2O_2 and O_2^- is widespread owing to their high ability to diffuse across the cell membrane and high generation rate in the mitochondria, respectively. Catalase (CAT), peroxidase (POD), and superoxide dismutase (SOD) are the major intrinsic enzymes that regulate H_2O_2 and O_2^- to avoid oxidative stress. To demonstrate the CAT-like-, POD-like-, and SOD-like enzymatic activities of the Pt NPs, three classical chemical reactions were performed.

CAT catalyzes the reduction of H_2O_2 to H_2O and O_2. The absorbance of H_2O_2 at 240 nm was negatively correlated with the CAT-like activity of the Pt NPs. As shown in Fig. 1C, H_2O_2 was relatively stable in the absence of Pt NPs for 90 min (black lines). The amount of H_2O_2 decreased quickly in the presence of Pt NPs. Compared with the low dose (0.4 mM, cyan line), the high dose of Pt NPs (4 mM, blue line) exhibited higher CAT-like activity.

POD catalyzes the decomposition of H_2O_2 to H_2O, during which process the colorless TMB is oxidized to blue. Oxidized TMB exhibited a strong absorption at 562 nm. Absorbance was positively correlated with POD-like activity. TMB alone (black line) and TMB with H_2O_2 (cyan line) seemed to have the same absorbance during the 30 min test. When Pt NPs were added to the mixture of TMB and H_2O_2, the absorbance increased quickly in a concentration-dependent manner (Fig. 1D), confirming that the Pt NPs possessed POD-like activity.

SOD catalyzes the dismutation of O_2^- into O_2 and H_2O_2. In the

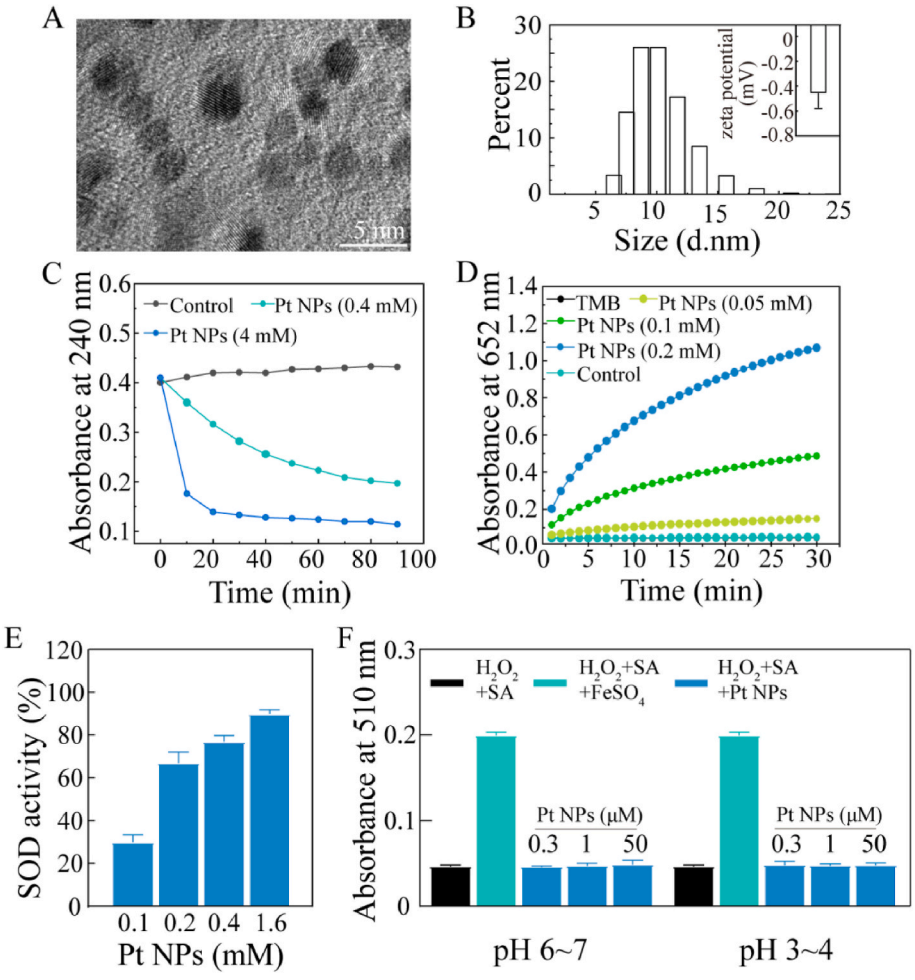

Fig. 1. Physical and chemical characterizations of Pt NPs. (A) TEM image of Pt NPs. (B) The size distribution of Pt NPs. The insert was zeta potential of Pt NPs. (C) CAT-like activity: time-dependent UV–visible absorption at 240 nm of H_2O_2 solution after incubating with Pt NPs. H_2O_2 alone was considered as control. (D) POD-like activity: time-dependent UV–visible absorption at 652 nm of the solution after incubating with Pt NPs. TMB alone (black) and TMB mixing with H_2O_2 (cyan) as control. (E) SOD-like activity: concentration-dependent SOD activity of Pt NPs at increased concentrations. (F) No Fenton-reaction-like activity of Pt NPs: H_2O_2 mixing with SA, $FeSO_4$ or without $FeSO_4$ was used as control, respectively. The mixture of H_2O_2, SA and various concentrations of Pt NPs (blue) was used for testing. The Pt NPs were pre-incubation wiht PBS (pH 6–7) or acetate buffer (pH 3–4).

absence of Pt NPs, O_2^- generated by the mixture of the NBT working solution and the starting solution provided in the kit oxidized NBT to turn blue. In the presence of Pt NPs, O_2^- was quenched, which inhibited the oxidation of NBT. As shown in Fig. 1E, the SOD-like activity increased with higher concentrations of Pt NPs.

We also determined whether Pt NPs elicited the Fenton reaction. In the Fenton reaction, free metal ions, such as Fe^{2+}, catalyze H_2O_2 to form destructive•OH. As shown in Fig. 1F, Fe^{2+} catalyzed H_2O_2 to produce •OH, followed by the oxidation of SA. The oxidized SA exhibited specific absorption at 510 nm. There was no change in the absorbance when replacing $FeSO_4$ with Pt NPs. NPs undergo lysosomal encapsulation within the cells. Therefore, Pt NPs were added to acetate buffer (pH 3–4) to mimic lysosomal conditions, followed by a repeated Fenton reaction. The results (Fig. 1F) indicated that the Pt NPs did not undergo the Fenton reaction even under acidic conditions. Thus, these experiments showed that Pt NPs possessed enzymatic activities of CAT, POD and SOD, but did not release •OH through the Fenton reaction.

4.3. Effect of Pt NPs on rescuing oxidative stressed cells

A cytotoxicity assay was performed to assess the biocompatibility of the Pt NPs. There was no obvious change in cell viability with a concentration range from 0 to 400 μM, indicating the biosafety of Pt NPs (Fig. 2A and B). H_2O_2 is used to establish cellular models of oxidative stress. Cell viability was significantly reduced to approximately 80% in the vehicle group. This reduction was reversed after post-treated with Pt NPs, especially 3 and 10 nM of Pt NPs ($p < 0.05$). The rescue effect was enhanced by increasing the concentration of Pt NPs (Fig. 2C). Crystal violet staining was performed to visualize this rescue effect. The cells post-treated with Pt NPs appeared much denser and more stretched than those in the vehicle group (Fig. 2D and E). The relative cell number of the vehicle group reduced to about 66% while that was improved in 1 nM (mean 76) and 3 nM (mean 81.9) of Pt NPs group ($p < 0.05$). Therefore, Pt NPs can improve cell viability, morphology, and cell number of the oxidative stressed cells.

Because O_2^- is one of the most important ROS, MitoSox Red was firstly used for the imaging of O_2^-. The results (Fig. 3A) showed a significant reduction in O_2^- levels in the Pt NPs group when compared with those in the vehicle group. DCFH-DA was used to image total ROS in the cells. Cells post-treated with Pt NPs showed fewer ROS fluorescent cell spots than that in the vehicle (Fig. 3B). ROS levels were quantified by flow cytometry and the results (Fig. 3C) showed that the ROS level of the vehicle cells (63%) was significantly higher than that of the normal cells (47.3%). This aberrant ROS production was reduced by treatment with Pt NPs; in particular, treatment with 3 nM Pt NPs reduced it to 42%. Thus, the ROS imaging results indicate that Pt NPs can effectively scavenge intracellular ROS.

As we know, autophagy is one of the important events in pro-death and pro-survival signaling cascade, which is characterized by the formation of autophagosomes and interaction with the lysosome. The progressive accumulation of cellular damage due to stressors, such as oxidative stress, inflammation, and endoplasmic reticulum stress, induces an increase in autophagy to degrade damaged organelles, protein aggregates, and lipid droplets. MDC is an autofluorescent dye that specifically stains autophagosomes. As shown in Fig. 3D and E, autophagy was significantly increased both in the vehicle and Pt NPs group (approximately 2-fold, $p < 0.05$). There were no apparent differences between the vehicle and Pt NPs groups. Results from the TUNEL assay (Fig. 3F and G) displayed that percent of $TUNEL^+$ cells was approximately 10% in vehicle group while that of the 3 nM Pt NPs group was less than 5% ($p < 0.05$). There was an obvious decrease in the number of $TUNEL^+$ cells in the Pt NPs group, especially in the 3 nM group when compared with the vehicle group.

Given the results of cell viability, crystal violent staining, autophagy-staining and TUNEL assays, we knew that although there was a similar increase of autophagy in vehicle and Pt NPs groups, more survived cells

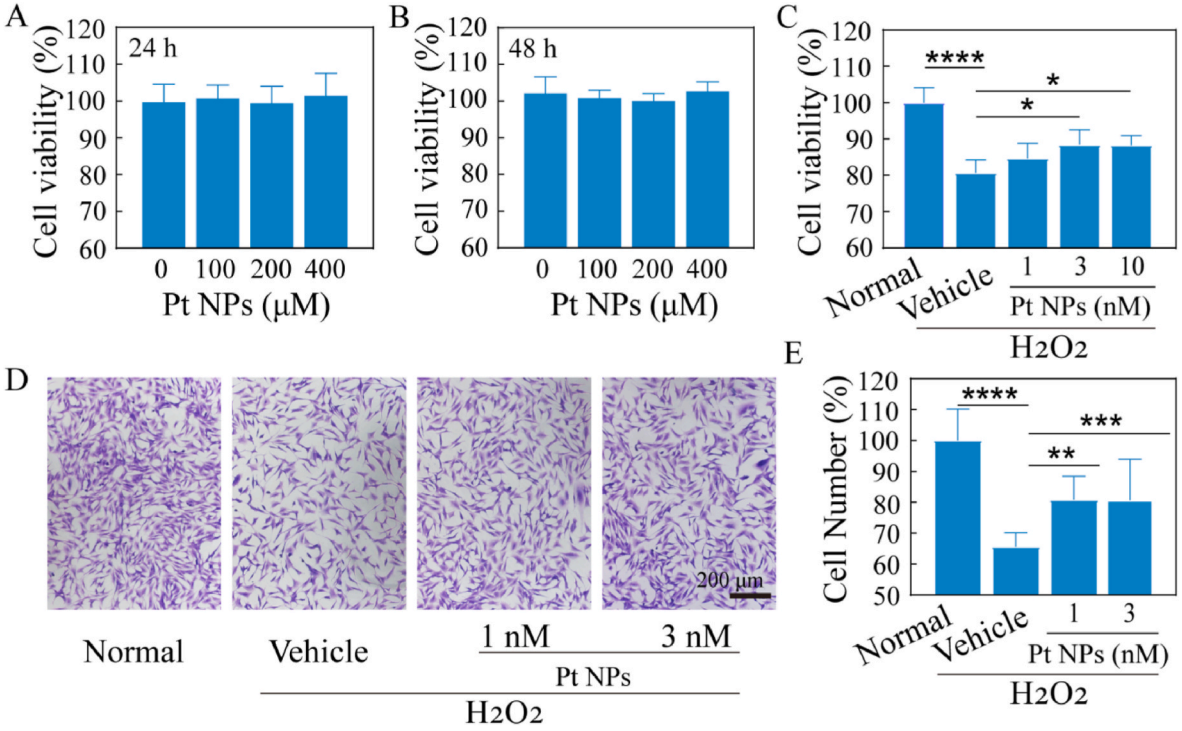

Fig. 2. The protective effect of Pt NPs on H_2O_2-induced oxidative damage *in vitro*. (A) and (B) The evaluation of viability after cells incubation with different concentrations of Pt NPs for 24 h and 48 h, respectively. (C) Protective effect of Pt NPs on viability of cells after treatment with H_2O_2. (D) Crystal violet staining images for each group to observe cell morphology and density. (E) Cell number statistics for each group based on crystal violet staining. H_2O_2 was used to induce oxidative stress in the cells. Cells post-treated with vehicle were named as vehicle. The cells with no H_2O_2 and no treatment were set as normal group. Data are expressed as the mean ± SD, $n \geqq 4$. One-way ANOVA were used for comparisons with vehicle. ****$p < 0.0001$; ***$p < 0.001$; **$p < 0.01$; *$p < 0.05$.

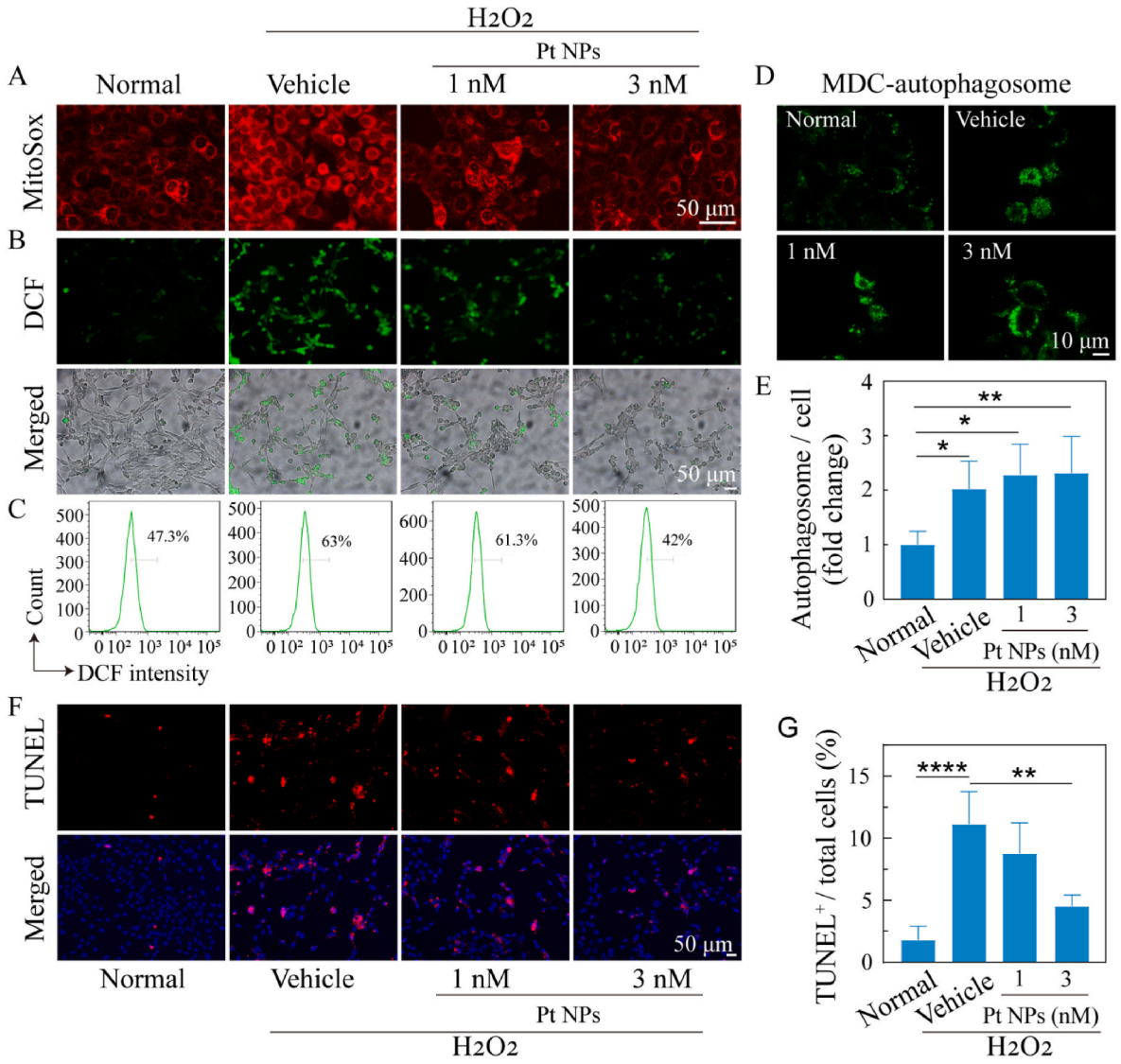

Fig. 3. Antioxidant and protective effects of Pt NPs on 661W cells. (A) MitoSox Red staining images of cells after different treatments. Scale bars, 50 μm. (B) DCF staining images of cells after different treatments. Scale bars, 50 μm. (C) The cytoflow analysis of DCF-stained cells for each group. (D) MDC-staining images of autophagosomes in cells after different treatments (green, autophagosome). Scale bars, 10 μm. (E) The statistics of MDC-fluorescent signal for each group are plotted. (F) TUNEL staining images of cells after different treatments (red, TUNEL positive). Scale bars, 50 μm. (G) The statistics of TUNEL positive cells are plotted. H_2O_2 was used to induce oxidative stress in cells. Cells post-treated with vehicle were named as vehicle. The cells with no H_2O_2 and no treatment were set as normal group. Data are expressed as the mean ± SD, n ≧ 4. One-way ANOVA were used for comparisons with vehicle. ROS, Reactive oxygen species. MDC, Monodansylcadaverine. ****$p < 0.0001$; ***$p < 0.001$; **$p < 0.01$.

in the Pt NPs groups than that of the vehicle. It's known that increased autophage benefites the survival of stressed cells, but excessive autophagy also lead to apoptosis. So we thought that autophagy acts as pro-apoptosis in the vehicle group while as pro-survival in the Pt NPs group because of different levels of intracellular ROS [22]. Therefore, we speculated that there might be other potential alterations in the Pt NPs treated cells.

4.4. *Pt NPs protect retina against oxidative stress in vivo*

Initially, the biosafety of Pt NPs in the retina was assessed by intravitreal injection. The results of OCT and H&E staining assays showed no obvious alterations in the structure and thickness of the retina (Supporting Fig. 3). The LIRD mouse model was used for *in vivo* assessments. The exposure of intense blue light caused rapid death of numerous PRs and disruptions of the retinal structure and function. To verify the antioxidant activities of Pt NPs in the retina, retinas were collected and processed to test the contents of MDA and GSH. MDA is a lipid peroxidation marker of oxidative stress and GSH is commonly considered as a key reductive small molecule. As shown in Fig. 4A and B, MDA significantly increased to approximately 1.27-fold and GSH decreased to 0.9-fold in the vehicle group, indicating the occurrence of oxidative stress. Post-treatment with Pt NPs (1 μM) distinctly reduced the MDA content (mean = 0.98, $p < 0.05$) and increased the GSH content (mean = 0.97, $p < 0.05$) when compared to the vehicle. In addition, the results of DHE staining on frozen section of retina (Supporting Fig. 4) displayed obvious decrease of oxidative stress in the Pt NPs-treated group when compared to the vehicle group.

The ERG is a sensitive method for testing the visual function of the retina. Generally, the A-wave represents the function of PRs and the B-wave refers to the activity of cells distal to the PRs, including bipolar cells. Moreover, completion of the transmission emanating from the PRs is necessary to generate a normal B-wave. As shown in Fig. 4C, D, and 4E, the ERG results showed that the amplitude of A-wave and B-wave of

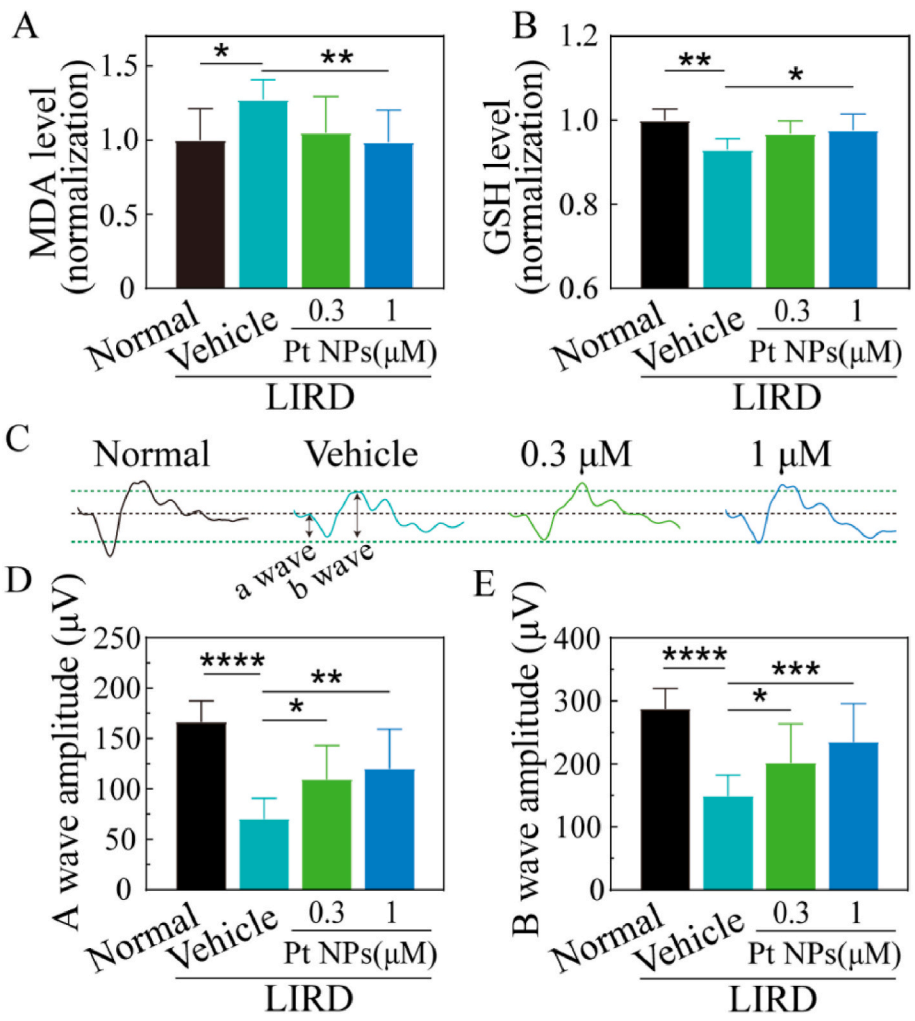

Fig. 4. Pt NPs protect retina against oxidative stress and rescue retina function in a dose-dependent manner. (A) MDA (a marker of oxidative stress) level in each group. (B) GSH (an important antioxidant) level in each group. (C) Representative profile of ERG for each group. Black and green dashed lines are served as auxiliary line. (D) and (E) The statistics of amplitude of A wave and B wave for each group, respectively. Intense blue light was used to induce retinal degeneration model. The mice post-treated with vehicle were named as vehicle. The mice with no light-induction and injection of vehicle were considered as normal group. Data are expressed as the mean ± SD, n ≧ 10. One-way ANOVA was used for comparisons with vehicle. ****$p < 0.0001$; ***$p < 0.001$; **$p < 0.01$, *$p < 0.05$. MDA,Malondialdehyde. GSH, Glutathione. ERG, Electroretinogram.LIRD, light-induced retinal degeneration.

the vehicle group were reduced to 70 mV and 148 mV, respectively. Post-treatment with Pt NPs, especially 1 μM group, mitigated the reduction of amplitude both in the A-wave (mean = 120.3) and B-wave (mean = 234). These results suggested that Pt NPs effectively protected PRs from oxidative damage.

A TUNEL assay was performed to visualize the therapeutic effect of Pt NPs on apoptosis of PRs in the retina. Fig. 5A showed there was a large number of $TUNEL^+$ cells in the retina of vehicle group. It's noteworthy that both of the two concentrations (0.3 and 1 μM) of Pt NPs significantly decreased the number of $TUNEL^+$ cells. The $TUNEL^+$ cells were mainly localized in the ONL, which is composed of photoreceptor nuclei. Therefore, it is reasonable to conclude that Pt NPs can protect PRs from oxidative stress induced apoptosis.

To assess the overall therapeutic effect of Pt NPs on the light-induced retina, OCT was used to obtain cross-sectional images (Fig. 5C) to measure the thickness of the ONL, starting at a distance of 1000 μm from the optic nerve (ON) and proceeding in the superior and inferior directions with an interval of 100 μm (Fig. 5D). Because ONL thickness is directly proportional to the number of PR nuclei, the thickness of each position was plotted to demonstrate the loss of PRs at different positions (Fig. 5E). Light-induced retina in the vehicle group showed an obvious reduction of ONL thickness (low than 30 μm), while post-treatment with Pt NPs of both two concentrations improved the thickness of ONL in all of the measured positions. Thus, the OCT results indicated the protective effects of Pt NPs in reducing the loss of PRs.

H&E staining of the retina was used for histological analysis to further validate the protective effects of the Pt NPs. As shown in Fig. 6, in contrast to the vehicle group, Pt NPs not only mitigated the loss of cells in the ONL but also improved the structure ordering of the IS and OS. In addition, the RGC lost was also significantly reduced in the Pt NPs group. Comparing the reduction of the thickness of the ONL, IS, and OS, we found that the OS seemed to be more sensitive to oxidative damage due to the largest reduction in thickness. There was about one fold increase of the thickness of OS in the Pt NPs (1 μM) group when compared to the vehicle group. Thus, the H&E staining results validated Pt NPs effectively protected RPs from oxidative damage.

4.5. The occurrence of metabolic reprogramming revealed by RNA sequencing

RNA sequencing was performed to investigate other beneficial alterations in Pt NP-treated retinas. The differentially expressed genes in the three groups are displayed in Fig. 7A, and the top 20 KEGG pathways (Pt NPs group vs. vehicle) are displayed in Fig. 7B. It is noteworthy that the metabolic pathway occupied top 1 and other metabolism-related pathways were also listed in the top 20, including oxidative phosphorylation, the mTOR signaling pathway, the MAPK signaling pathway, the PI3K-Akt signaling pathway, and the FoxO signaling pathway, indicating the effects of Pt NPs on retinal metabolism. Among these pathways, FoxO is considered as an important metabolic regulator that is activated by multiple changes, including growth factor deprivation, metabolic stress (starvation), and oxidative stress [23]. Additionally, FoxO activity is negatively regulated by multiple upstream pathways, including the mTOR, MAPK, and PI3K-Akt pathways [24,25]. Therefore,

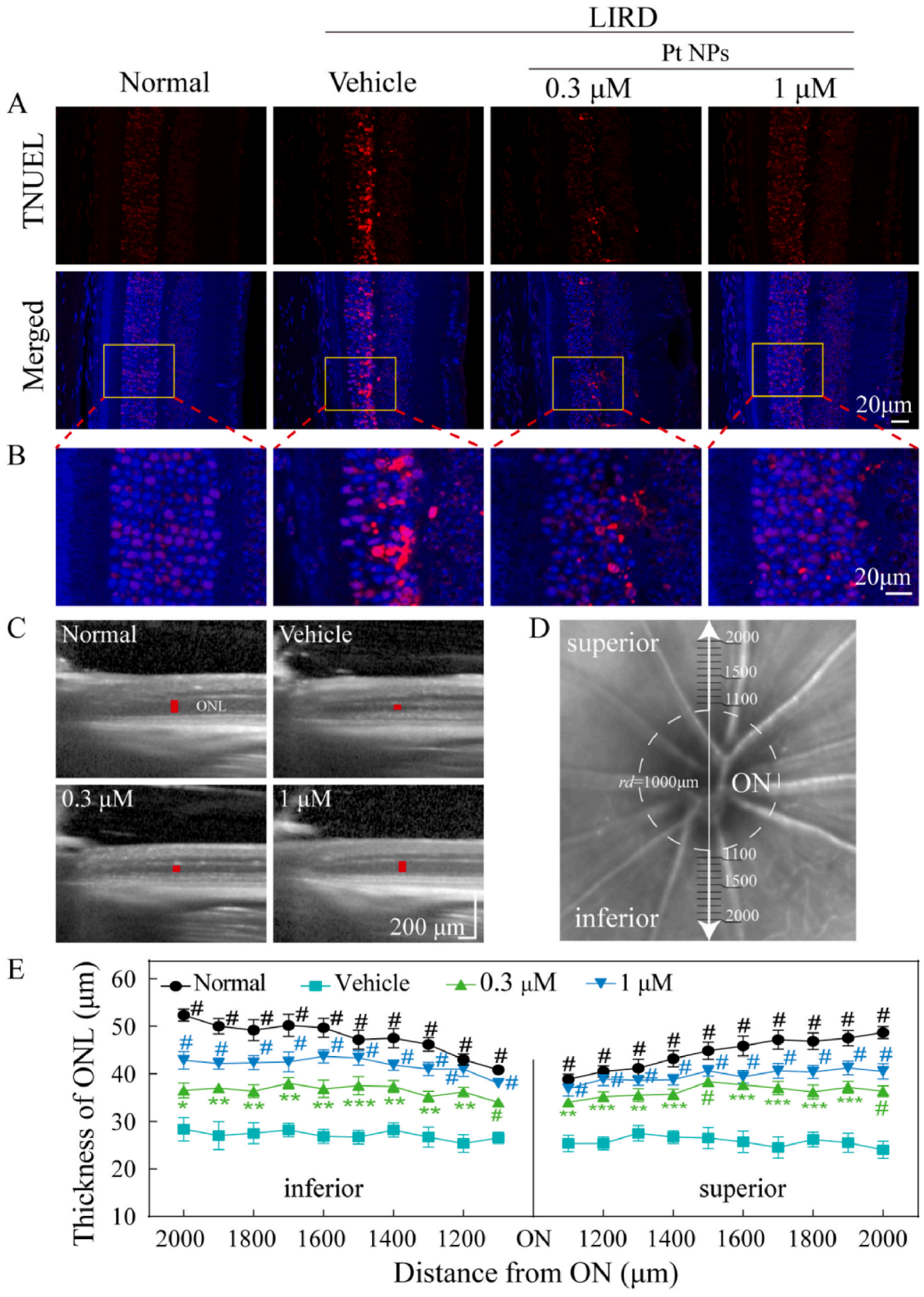

Fig. 5. Pt NPs protect PRs from light-induced oxidative damage. (A) Pt NPs reduced TUNEL^{+} cells in ONL of the retina. Scale bar, 20 μm. (B) Zoomed view of the region inside the box in the upper figures (red, TUNEL positive cells; blue, DAPI for nucleus). Scale bar, 20 μm. (C) Representative images of OCT for each group. The red lines indicated the thickness of ONL. (D) Schematic diagram of the method to measure the thickness of the ONL. (E) The thickness of the ONL at each position was plotted. ONL, outer nuclear layer. ON, optic nerve. LIRD mice that post-treated with vehicle were names as vehicle. Data are expressed as the mean ± SEM, n ≧ 10. One-way ANOVA were used for comparisons with vehicle. #$p < 0.0001$; ***$p < 0.001$; **$p < 0.01$. LIRD, light-induced retinal degeneration.

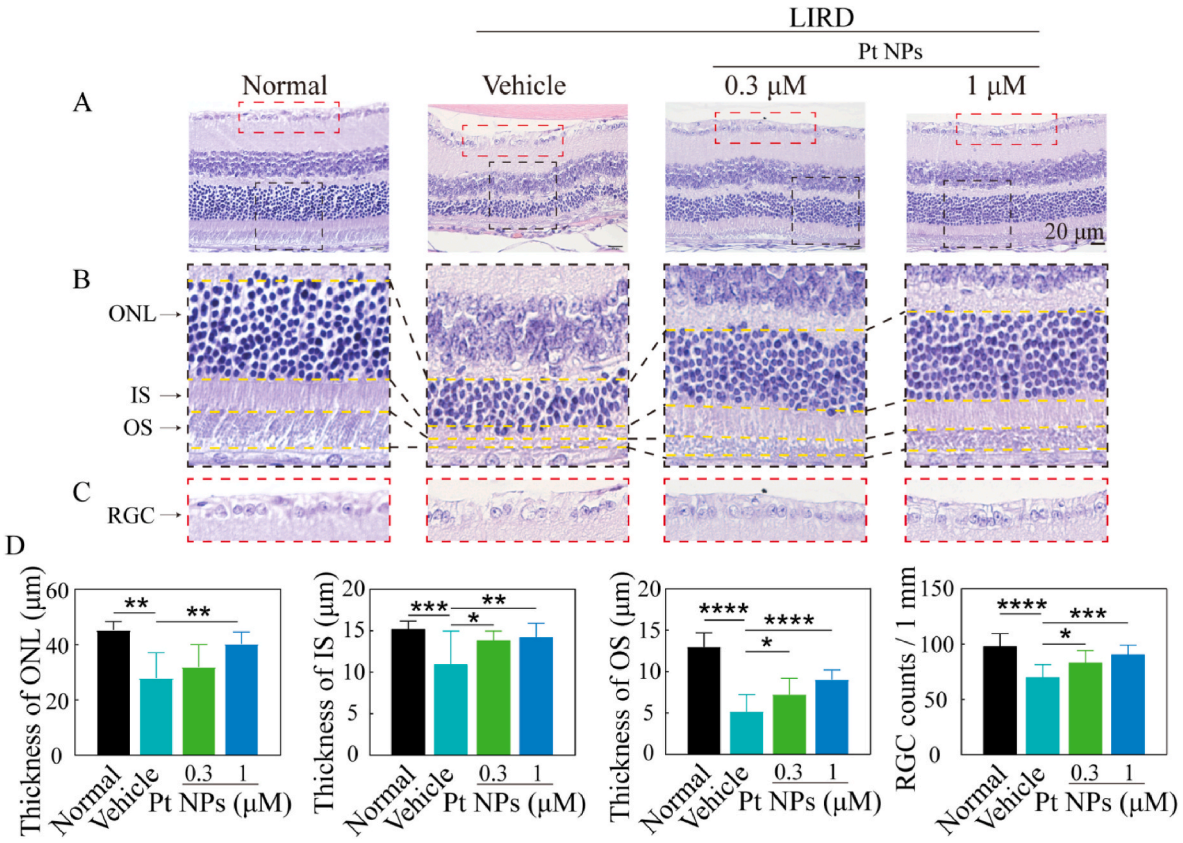

Fig. 6. Post-treatment with Pt NPs protected the structure of light-induced retina. (A) H&E staining images of the retina for each group. (B) Enlarged view of the region inside the black box in (A). (C) Enlarged view of the region inside the red box in (A). (D) The statistics of ONL, IS, OS and RGC for each group. LIRD mice that post-treated with vehicle were named as vehicle. Data are expressed as the mean ± SD, n ≧ 10. One-way ANOVA were used for comparisons with vehicle. ****p < 0.0001; ***p < 0.001; **p < 0.01; *p < 0.05. RGC, retinal ganglion cell layer. ONL, outer nuclear layer. IS, inner segment of the photoreceptors. OS, outer segment of the photoreceptors. LIRD, light-induced retinal degeneration.

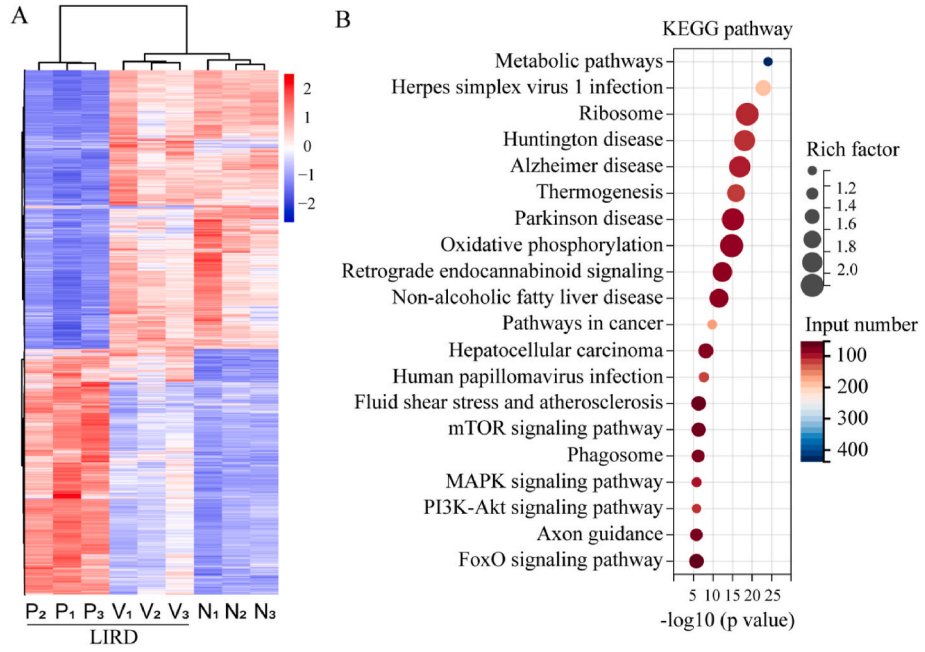

Fig. 7. Results of RNA sequencing. (A) The differential genes of normal (N), vehicle (V) and Pt NPs group (P). LIRD mice that post-treated with vehicle were named as vehicle. There was 3 replicates in each group. (B) The top 20 KEGG pathway (by p value) enriched by differential genes (Pt NPs vs. vehicle group). LIRD, light-induced retinal degeneration.

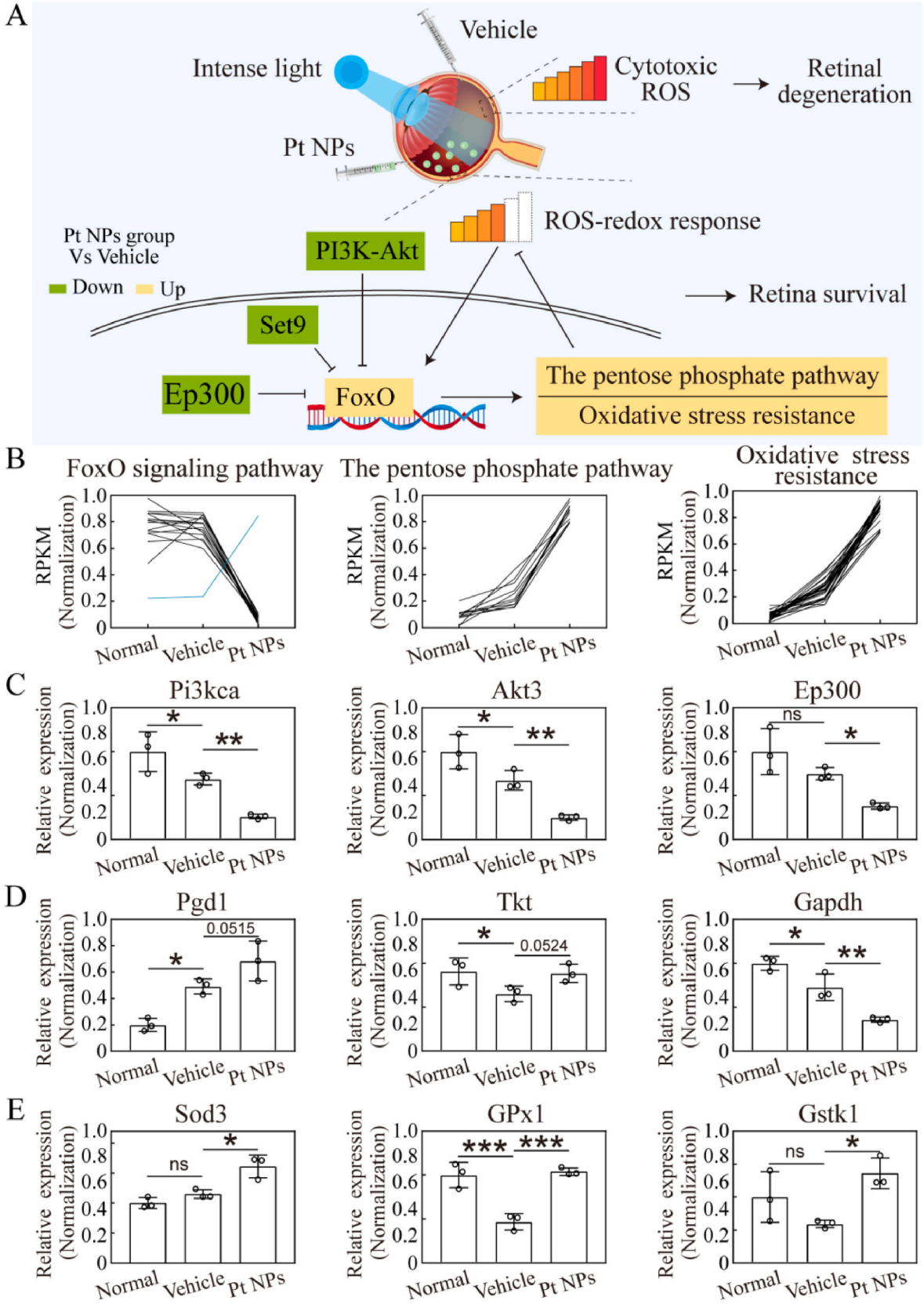

Fig. 8. Important pathways and genes for retina survival in the Pt NPs group. (A) Illustration of mechanism for this study. In the vehicle group, cytotoxic ROS induced by intense light caused retinal degeneration. In the Pt NPs group, cytotoxic ROS was reduced by Pt NPs, activating FoxO pathway to regulate downstream pathway. (B) The normalization of RPKM for the genes that enriched on pathway, based on the result of RNA sequencing. (C) The mRNA expression of 3 key genes of the FoxO pathway. (D) The mRNA expression of 3 key genes of the pentose phosphate pathway. (E) The mRNA expression of 3 key genes of the oxidative stress resistant pathway. Four retinas from different mouse belonging to the same group were pooled and considered as one sample, and each group had 3 replicate samples ($n = 3$). Data are expressed as the mean ± SD. One-way ANOVA were used for comparisons with vehicle. ***$p < 0.001$; **$p < 0.01$; *$p < 0.05$.

the upregulation of the FoxO pathway (Fig. 8A) may be linked to the effects of Pt NPs on metabolism.

PI3K-Akt pathway, Set9 and Ep300 are well-known negative regulators of the FoxO pathway [26]. In this study, the cytotoxic ROS generated by light-induction caused retinal degeneration in the vehicle group, whereas cytotoxic ROS was reduced to redox response level in the presence of Pt NPs. The results of RNA sequencing revealed that the FoxO pathway was activated to further regulate downstream in the Pt NPs treated retina (Fig. 8A). As reported, the FoxO pathway is involved in the regulation of multiple pathways, including the pentose phosphate pathways and oxidative stress resistance [23], both of which were upregulated in the Pt NPs-treated retinas (Fig. 8B). The expression of these genes were upregulated amd limited the accumulation of ROS and their derivatives.

Quantitative PCR was performed to validate the results of the RNA sequencing. As shown in Fig. 8C, the mRNA expression of Pi3kca, Akt3 and Ep300 was significantly reduced in the Pt NPs group. Under this condition the FoxO was translocated into nucleus, activating downstream regulation. As shown in Fig. 8D, the mRNA expression of Pgd1 and Tkt was upregulated and Gapdh was downregulated. This alteration rerouted glucose flux from glycolysis into the pentose phosphate pathway, alleviating oxidative stress through generating more NADPH. This metabolic reprogramming is one of the primary defenses against oxidative stress. Sod3, Gpx1 and Gstk1 played important role in anti-oxidative network. As shown in Fig. 8E, the mRNA expression of these 3 genes in the Pt NPs group were significantly upregulated when compared to that of the vehicle group. Therefore, it was confirmed that metabolic reprogramming occurred in the Pt NPs treated retina to further regulated homeostasis.

5. Discussions

In this study, we demonstrated that Pt NPs could effectively reduce excessive ROS in LIRD model and protected the retina from oxidative damage. The results of *in vitro* experiment indicated that Pt NPs effectively reduced intracellular ROS, decreased the number of apoptotic cells and increased cell viability, while in the animal model of LIRD, Pt NPs was proved to alleviate light-induced oxidative stress and ameliorate retinal degeneration. The results of RNA sequencing further indicated that Pt NPs may promote retinal survival by restoring redox balance through metabolic reprogramming. We also validated that Pt NPs possessed CAT, POD and SOD-like activities, but without the harmful Fenton reaction as iron ions. All these results suggested that Pt NPs might be a promising anti-oxidant for retinal degeneration.

Targeting oxidative stress is promising for the treatment of PRs degeneration, because PRs are susceptible to oxidative stress due to their active metabolism and high-energy demand. In the last two decades, numerous studies have focused on antioxidant compounds derived from comestible foods, such as lutein, zeaxanthin, vitamins, and DHA [27,28]. Although these compounds have exhibited therapeutic potential in preclinical studies, the outcomes of clinical trials are disappointing [29–31]. Pt NPs, which are potent antioxidants with high stability, have been used in the treatment of oxidation-related diseases of the nervous system and ischemia-reperfusion injury [16]. Since Pt NPs can stay in the cells for a long period, they will be useful as long as they are there. In this study, Pt NPs were introduced to protect PRs from oxidative stress-induced degeneration and to provide a new therapeutic strategy for retinal diseases.

Faced with intense light stimuli, PRs require a more active metabolism to meet the energy demand for impairment and renewal to survive [32]. However, excessive ROS generated by metabolism can block metabolism, leading to failure of survival [5,33]. We hypothesized that the key to rescuing light-induced retinas is by improving the removal of ROS generated by active metabolism. In this study, Pt NPs assisted the light-induced retina by removing excess ROS, which allowed the retina to adopt inherently adaptive mechanisms to maintain homeostasis through metabolic reprogramming. In the presence of Pt NPs, a new reductive-oxidative homeostasis was established in the retina, with high generation and removal levels of ROS.

Although many studies have shown the potential use of Pt NPs as anti-oxidative nanomedicines in the skin [18,34], lung [35,36] and brain diseases [37,38], the effects of Pt NPs on metabolism have not yet been addressed. We found that although the autophagy was increased both in the vehicle and Pt NPs groups, more cells survived only in the Pt NPs groups, suggesting there may be other potentially beneficial alterations existing in the Pt NPs-treated cells except for reduced oxidative stress. Therefore, RNA sequencing was performed to explore the potential mechanism. The RNA sequencing results implied that there was be a relationship between Pt NPs and metabolism. Among the top 20 KEGG pathways (Pt NPs group vs. vehicle), metabolic pathways were the most abundant. Importantly, the FoxO pathway, which is a key metabolism-related pathway, was also identified among the top 20 KEGG pathways. The FoxO pathway is activated in response to a variety of stressors, such as lack of nutrition, energy, and oxidative stress [23]. The results of RNA sequencing also showed that downstream pathways of FoxO were upregulated in the Pt NP-treated retinas, including oxidative stress resistant and the pentose phosphate pathway. The upregulation of the pentose phosphate pathway indicated the metabolic rerouting of glucose flux. In addition, platinum-based chemotherapy has been reported to affect serine metabolism in ovarian cancer, despite an unidentified mechanism [39]. Therefore, it can be speculated that acute oxidative stress was reduced to a hypolethal level by Pt NPs, under which condition the FoxO was activated to regulate multiple metabolic pathways and returned to regulate ROS. In particular, the upregulated pentose phosphate pathway may play a critical role in this process by providing sufficient NADPH for the reductive system and intermediates for biosynthesis [40,41], contributing to the survival of the retina.

In conclusion, our results indicate that Pt NPs are promising candidate nanozymes for the treatment of oxidative stress-related retinal diseases owing to their potent antioxidant capacity, and deserve further investigations, including targeted delivery to photoreceptors, long-term cytotoxicity and pharmacokinetics of Pt NPs in the eyes.

Declaration of competing interest

All authors disclosed no relevant relationships.

Data availability

The data that has been used is confidential.

Acknowledgments

The authors are thankful to Department of Pathology, Tianjin Medical University Eye Hospital for providing laboratory assistance. This research was supported by National Natural Science Foundation of China (81800880, 81870675 and 82171085).

Appendix A. Supplementary data

Supplementary data to this article can be found online at https://doi.org/10.1016/j.redox.2023.102836.

References

[1] M.W. Country, Retinal metabolism: a comparative look at energetics in the retina, Brain Res. 1672 (2017) 50–57.
[2] X. Shi, P. Li, H. Liu, V. Prokosch, Oxidative stress, vascular endothelium, and the Pathology of neurodegeneration in retina, ANTIOXIDANTS-BASEL 11 (2022).
[3] Y. Ruan, S. Jiang, A. Musayeva, A. Gericke, Oxidative stress and vascular dysfunction in the retina: therapeutic strategies, ANTIOXIDANTS-BASEL 9 (2020).
[4] T. Leveillard, J.A. Sahel, Metabolic and redox signaling in the retina, Cell. Mol. Life Sci. 74 (2017) 3649–3665.

[5] D.S. Narayan, G. Chidlow, J.P. Wood, R.J. Casson, Glucose metabolism in mammalian photoreceptor inner and outer segments, Clin. Exp. Ophthalmol. 45 (2017) 730–741.
[6] W.W. Pan, T.J. Wubben, C.G. Besirli, Photoreceptor metabolic reprogramming: current understanding and therapeutic implications, COMMUN BIOL 4 (2021) 245.
[7] Y. Du, A. Veenstra, K. Palczewski, T.S. Kern, Photoreceptor cells are major contributors to diabetes-induced oxidative stress and local inflammation in the retina, P NATL ACAD SCI USA 110 (2013) 16586–16591.
[8] H.P. Hammes, Diabetic retinopathy: hyperglycaemia, oxidative stress and beyond, Diabetologia 61 (2018) 29–38.
[9] S. Beatty, H. Koh, M. Phil, D. Henson, M. Boulton, The role of oxidative stress in the pathogenesis of age-related macular degeneration, Surv. Ophthalmol. 45 (2000) 115–134.
[10] T. Masuda, M. Shimazawa, H. Hara, Retinal diseases associated with oxidative stress and the effects of a free radical scavenger (edaravone), Oxid. Med. Cell. Longev. (2017), 9208489, 2017.
[11] G.D. Calderon, O.H. Juarez, G.E. Hernandez, S.M. Punzo, Z.D. De la Cruz, Oxidative stress and diabetic retinopathy: development and treatment, Early Years Educat. 31 (2017) 1122–1130.
[12] D. Pedone, M. Moglianetti, E. De Luca, G. Bardi, P.P. Pompa, Platinum nanoparticles in nanobiomedicine, Chem. Soc. Rev. 46 (2017) 4951–4975.
[13] T. Kim, T. Hyeon, Applications of inorganic nanoparticles as therapeutic agents, Nanotechnology 25 (2014), 12001.
[14] H. Xu, S. Li, Y.S. Liu, Nanoparticles in the diagnosis and treatment of vascular aging and related diseases, SIGNAL TRANSDUCT TAR 7 (2022) 231.
[15] H. Wei, E. Wang, Nanomaterials with enzyme-like characteristics (nanozymes): next-generation artificial enzymes, Chem. Soc. Rev. 42 (2013) 6060–6093.
[16] J. Mu, C. Li, Y. Shi, G. Liu, J. Zou, D.Y. Zhang, C. Jiang, X. Wang, L. He, P. Huang, Y. Yin, X. Chen, Protective effect of platinum nano-antioxidant and nitric oxide against hepatic ischemia-reperfusion injury, Nat. Commun. 13 (2022) 2513.
[17] H. Gehrke, J. Pelka, C.G. Hartinger, H. Blank, F. Bleimund, R. Schneider, D. Gerthsen, S. Brase, M. Crone, M. Turk, D. Marko, Platinum nanoparticles and their cellular uptake and DNA platination at non-cytotoxic concentrations, Arch. Toxicol. 85 (2011) 799–812.
[18] S. Shibuya, Y. Ozawa, K. Watanabe, N. Izuo, T. Toda, K. Yokote, T. Shimizu, Palladium and platinum nanoparticles attenuate aging-like skin atrophy via antioxidant activity in mice, PLoS One 9 (2014), e109288.
[19] M. Gulino, S.D. Santos, A.P. Pego, Biocompatibility of platinum nanoparticles in brain ex vivo models in physiological and pathological conditions, FRONT NEUROSCI-SWITZ 15 (2021), 787518.
[20] M. Moglianetti, L.E.P. D, Platinum nanozymes recover cellular ROS homeostasis in an oxidative stress-mediated disease model, Nanoscale 8 (6) (2016) 3739–3752.
[21] T.D. Schmittgen, K.J. Livak, Analyzing real-time PCR data by the comparative C(T) method, Nat. Protoc. 3 (2008) 1101–1108.
[22] K.C. Chang, P.F. Liu, C.H. Chang, Y.C. Lin, Y.J. Chen, C.W. Shu, The interplay of autophagy and oxidative stress in the pathogenesis and therapy of retinal degenerative diseases, Cell Biosci. 12 (1) (2022).
[23] A. Eijkelenboom, B.M. Burgering, FOXOs: signalling integrators for homeostasis maintenance, Nat. Rev. Mol. Cell Biol. 14 (2013) 83–97.
[24] S. Papa, P.M. Choy, C. Bubici, The ERK and JNK pathways in the regulation of metabolic reprogramming, Oncogene 38 (2019) 2223–2240.
[25] R.A. Saxton, D.M. Sabatini, mTOR signaling in growth, metabolism, and disease, Cell 168 (2017) 960–976.
[26] G. Calissi, E.W. Lam, W. Link, Therapeutic strategies targeting FOXO transcription factors, Nat. Rev. Drug Discov. 20 (2021) 21–38.
[27] Q. Bian, S. Gao, J. Zhou, J. Qin, A. Taylor, E.J. Johnson, G. Tang, J.R. Sparrow, D. Gierhart, F. Shang, Lutein and zeaxanthin supplementation reduces photooxidative damage and modulates the expression of inflammation-related genes in retinal pigment epithelial cells, FREE RADICAL BIO MED 53 (2012) 1298–1307.
[28] J. Wu, E. Cho, W.C. Willett, S.M. Sastry, D.A. Schaumberg, Intakes of lutein, zeaxanthin, and other carotenoids and age-related macular degeneration during 2 decades of prospective follow-up, JAMA OPHTHALMOL 133 (2015) 1415–1424.
[29] A. Stahl, The diagnosis and treatment of age-related macular degeneration, DTSCH ARZTEBL INT 117 (2020) 513–520.
[30] J.R. Evans, J.G. Lawrenson, Antioxidant vitamin and mineral supplements for preventing age-related macular degeneration, COCHRANE DB SYST REV 7 (2017) CD253.
[31] H.J. Forman, H. Zhang, Targeting oxidative stress in disease: promise and limitations of antioxidant therapy, Nat. Rev. Drug Discov. 20 (2021) 689–709.
[32] D. Athanasiou, M. Aguila, D. Bevilacqua, S.S. Novoselov, D.A. Parfitt, M. E. Cheetham, The cell stress machinery and retinal degeneration, FEBS Lett. 587 (2013) 2008–2017.
[33] Y. Ozawa, Oxidative stress in the light-exposed retina and its implication in age-related macular degeneration, Redox Biol. 37 (2020), 101779.
[34] P. Konieczny, A.G. Goralczyk, R. Szmyd, L. Skalniak, J. Koziel, F.L. Filon, M. Crosera, A. Cierniak, E.K. Zuba-Surma, J. Borowczyk, E. Laczna, J. Drukala, E. Pyza, D. Semik, O. Woznicka, A. Klein, J. Jura, Effects triggered by platinum nanoparticles on primary keratinocytes, Int. J. Nanomed. 8 (2013) 3963–3975.
[35] X.L. Liu, X. Dong, S.C. Yang, X. Lai, H.J. Liu, Y. Gao, H.Y. Feng, M.H. Zhu, Y. Yuan, Q. Lu, J.F. Lovell, H.Z. Chen, C. Fang, Biomimetic liposomal nanoplatinum for targeted cancer chemophototherapy, Adv. Sci. 8 (2021), 2003679.
[36] S. Onizawa, K. Aoshiba, M. Kajita, Y. Miyamoto, A. Nagai, Platinum nanoparticle antioxidants inhibit pulmonary inflammation in mice exposed to cigarette smoke, Pulm. Pharmacol. Ther. 22 (2009) 340–349.
[37] Z. Elmazoglu, H. Kayhan, A. Santamaria, E. Rangel-Lopez, P.K. Ugur, A. Ceylan, M. Aschner, C. Karasu, Platinum nanoparticles protect against lipopolysaccharide-induced inflammation in microglial BV-2 cells via decreased oxidative damage and increased phagocytosis, Neurochem. Res. 46 (2021) 3325–3341.
[38] E. De Luca, D. Pedone, M. Moglianetti, D. Pulcini, A. Perrelli, S.F. Retta, P. P. Pompa, Multifunctional Platinum@BSA-rapamycin nanocarriers for the combinatorial therapy of cerebral cavernous malformation, ACS Omega 3 (2018) 15389–15398.
[39] T. Van Nyen, M. Planque, L. van Wagensveld, J. Duarte, E.A. Zaal, A. Talebi, M. Rossi, P.R. Korner, L. Rizzotto, S. Moens, W. De Wispelaere, R. Baiden-Amissah, G.S. Sonke, H.M. Horlings, G. Eelen, E. Berardi, J.V. Swinnen, C.R. Berkers, P. Carmeliet, D. Lambrechts, B. Davidson, R. Agami, S.M. Fendt, D. Annibali, F. Amant, Serine metabolism remodeling after platinum-based chemotherapy identifies vulnerabilities in a subgroup of resistant ovarian cancers, Nat. Commun. 13 (2022) 4578.
[40] J.S. Joyal, M.L. Gantner, L. Smith, Retinal energy demands control vascular supply of the retina in development and disease: the role of neuronal lipid and glucose metabolism, Prog. Retin. Eye Res. 64 (2018) 131–156.
[41] A. Perl, R. Hanczko, T. Telarico, Z. Oaks, S. Landas, Oxidative stress, inflammation and carcinogenesis are controlled through the pentose phosphate pathway by transaldolase, Trends Mol. Med. 17 (2011) 395–403.